Journal of Scientific Computing, Vol. 4, No. 3, 1989

Efficient Removal of Boundary-Divergence Errors in Time-Splitting Methods

A. G. Tomboulides,[1] M. Israeli,[1,2] and G. E. Karniadakis[1]

Received September 8, 1989

A normal mode analysis is presented and numerical tests are performed to assess the effectiveness of a new time-splitting algorithm proposed recently in Karniadakis *et al.* (1990) for solving the incompressible Navier–Stokes equations. This new algorithm employs high-order explicit pressure boundary conditions and mixed explicit/implicit stiffly stable time-integration schemes, which can lead to arbitrarily high-order accuracy in time. In the current article we investigate both the time accuracy of the new scheme as well as the corresponding reduction in boundary-divergence errors for two model flow problems involving solid boundaries. The main finding is that time discretization errors, induced by the nondivergent splitting mode, scale with the order of the accuracy of the integration rule employed if a proper rotational form of the pressure boundary condition is used; otherwise a first-order accuracy in time similar to the classical splitting methods is achieved. In the former case the corresponding errors in divergence can be completely eliminated, while in the latter case they scale as $\mathcal{O}(\nu \Delta t)^{1/2}$.

KEY WORDS: Splitting methods; normal mode analysis; incompressible flow.

1. INTRODUCTION

The numerical solution of unsteady *incompressible* Navier–Stokes equations that govern viscous flows requires a very different approach than the solution of the *compressible* equations as in the former case the constraint of a solenoidal velocity field introduces certain extra difficulties. The incompressibility constraint is ultimately tied to the pressure field, the role of which is to project the velocity from a space containing all solutions satisfying the momentum equation and appropriate boundary conditions to a restricted divergence-free space. The time-advancement of the incom-

[1] Mechanical and Aerospace Engineering, Princeton University, Princeton, New Jersey 08544.
[2] Permanent Address: Department of Computer Science, Technion University, Haifa, Israel.

0885-7474/89/0900-0291$06.00/0

pressible Navier–Stokes equations is therefore a key step in the discretization as it dictates the accuracy of the scheme. In addition, it determines the form of the system of equations to be solved and thus the degree of coupling between pressure and velocity fields. This coupling, in its turn, is indicative of the computational complexity involved in solving numerically the Navier–Stokes equations.

In the classical splitting method (Yanenko, 1971) the pressure satisfies a Poisson equation, separate from the velocity, and compatible Neumann boundary condition (BC). The exact form of this boundary condition is very important not only because it affects directly the overall accuracy of the scheme, but also because it determines the efficiency of the time-stepping algorithm. This is particularly true in simulations of unsteady flows in complex geometries, where a separately solvable second-order pressure equation is yet the only affordable approach. Splitting methods in conjunction with spectral and spectral element methods have been used with success in simulating highly unsteady flows in nonperiodic and very complex geometries (Orszag and Kells, 1980; Karniadakis *et al.*, 1988; Karniadakis and Triantafyllou, 1989). In these studies, splitting led to first-order accuracy, so that very small time steps were required in order to prevent significant time-differencing and splitting errors.

There have been a number of attempts in the last decade to modify the classical splitting method, so that high-order time accuracy could be obtained (Orszag *et al.*, 1986; Marcus, 1984; Kim and Moin, 1985; Zang and Hussaini, 1986).In the first article, a more systematic analysis is given, and various approaches are suggested to circumvent the spurious effects of splitting errors without any significant loss in efficiency or ease in implementation. An extension of that work was developed more recently in Karniadakis *et al.* (1990), where explicit high-order Neumann pressure boundary condition in conjunction with mixed explicit/implicit stiffly stable schemes were shown to lead to arbitrarily high-order time accuracy and good stability properties. Our work here is inspired primarily by the work in Karniadakis *et al.* (1990); our objective is to investigate how the splitting errors are induced in the splitting method and how they can be controlled or eliminated by using high-order time-accurate schemes.

The paper is organized as follows: In Section 2, we present a general normal mode analysis and compare the split semidiscrete equations with their continuous counterpart; we then apply the analysis to a two-dimensional problem with one periodic direction. In Section 3 we perform high-resolution numerical simulations to determine the overall time-accuracy and boundary-divergence errors in simple and complex geometries. Finally, in Section 4 we draw some conclusions based on the theoretical predictions and the numerical results.

2. NORMAL MODE ANALYSIS

2.1. Continuous Problem

We consider here Newtonian, incompressible flows with constant properties, which are governed by the Navier–Stokes equations written in the form

$$\frac{\partial \mathbf{v}}{\partial t} = -\nabla p + \nu \mathbf{L}(\mathbf{v}) + \mathbf{N}(\mathbf{v}) \qquad \text{in } \Omega \tag{2.1a}$$

subject to the incompressibility constraint

$$Q \equiv \nabla \cdot \mathbf{v} = 0 \qquad \text{in } \Omega \tag{2.1b}$$

where $\mathbf{v}(=u\hat{x}+v\hat{y}+w\hat{z})$ is the velocity vector, p is the static pressure, and ν is the kinematic viscosity. Here $\mathbf{L}$ and $\mathbf{N}$ represent the linear and nonlinear operators, respectively, and are defined as

$$\mathbf{L}(\mathbf{v}) \equiv \nabla^2 \mathbf{v} = \nabla(\nabla \cdot \mathbf{v}) - \nabla \times (\nabla \times \mathbf{v}) \tag{2.1c}$$

$$\mathbf{N}(\mathbf{v}) \equiv -\tfrac{1}{2}[\mathbf{v} \cdot \nabla \mathbf{v} + \nabla(\mathbf{v} \cdot \mathbf{v})] \tag{2.1d}$$

Taking the divergence of Eq. (2.1a) and dropping the nonlinear terms we obtain an equation for the pressure, given by

$$\nabla^2 p = 0 \tag{2.2a}$$

while taking the $\nabla \times \nabla$ of (2.1a) and using the incompressibility constraint [Eq. (2.1b)] we obtain

$$\left(\frac{\partial}{\partial t} - \nu \nabla^2\right) \nabla^2 \mathbf{v} = 0 \tag{2.2b}$$

To proceed we assume the existence of normal mode expansions in the form

$$\mathbf{v}(\mathbf{x}, t) = \sum_{i=1}^{\infty} e^{\sigma_i t} \mathbf{v}_i(\mathbf{x}) \tag{2.2c}$$

$$p(\mathbf{x}, t) = \sum_{i=1}^{\infty} e^{\sigma_i t} p_i(\mathbf{x}) \tag{2.2d}$$

where $\mathbf{v}_i(\mathbf{x})$ are the velocity normal modes known to have decay rates σ_i with nonpositive real parts, and $p_i(\mathbf{x})$ are the pressure modes. Substituting

above in Eqs. (2.2a) and (2.2b) we obtain the equations that the modes satisfy:

$$\nabla^2 p_i = 0 \tag{2.2e}$$

$$\left(\frac{\sigma_i}{\nu} - \nabla^2\right)\nabla^2 \mathbf{v}_i = 0 \tag{2.2f}$$

It follows from the above relations that the modes $p_i(\mathbf{x})$ are harmonic and satisfy a maximum principle theorem, and that the modes $\mathbf{v}_i$ have a harmonic part and an oscillatory part since $\mathrm{Re}[\sigma_i] \leqslant 0$.

2.2. Semidiscrete Problem

Using an implicit integration multistep scheme we can write the Stokes equation in a semidiscrete form as follows:

$$\frac{\gamma_0 \mathbf{v}^{n+1} - \sum_{q=0}^{J_i-1} \alpha_q \mathbf{v}^{n-q}}{\Delta t} = -\nabla \tilde{p}^{n+1} + \nu \sum_{q=0}^{J_i-1} \beta_q \nabla^2 (\mathbf{v}^{n+1-q}) \tag{2.3a}$$

where γ_0, α_q, and β_q are appropriate weight coefficients associated with the order J_i and the specific integration scheme employed. Assuming an amplification factor κ for the normal modes we can write that $(\mathbf{v}_i^n, p_i^n) = \kappa^n(\tilde{\mathbf{v}}_i, \tilde{p}_i)$ and thus we obtain

$$\left[\frac{\gamma_0 \kappa - P(\kappa)}{\Delta t}\right]\tilde{\mathbf{v}}_i = -\kappa \nabla \tilde{p}_i + \nu R(\kappa)\nabla^2 \tilde{\mathbf{v}}_i \tag{2.3b}$$

where we define the linear operators P, R as follows:

$$P(\kappa) = \sum_{q=0}^{J_i-1} \alpha_q \kappa^{-q} \quad \text{and} \quad R(\kappa) = \sum_{q=0}^{J_i-1} \beta_q \kappa^{1-q} \tag{2.3c}$$

Following a similar approach as before for the continuous problem we now obtain

$$\nabla^2 \tilde{p}_i = 0 \tag{2.3d}$$

$$\left(\frac{\sigma_i}{\nu} - \nabla^2\right)\nabla^2 \tilde{\mathbf{v}}_i = 0 \tag{2.3e}$$

$$\sigma_i = \frac{\gamma_0 \kappa - P(\kappa)}{\Delta t R(\kappa)} \tag{2.3f}$$

This expression is general and is valid for any mulistep method; for example (see Karniadakis *et al.*, 1990), for a Crank–Nicolson scheme the

appropriate coefficients are $\gamma_0 = 1$, $P = 1$, and $R = (\kappa + 1)/2$, and for a second-order stiffly stable scheme are $\gamma_0 = 3/2$, $P = 2 - 1/(2\kappa)$, and $R = \kappa$.

We find therefore by comparing with the results of the continuous case that the same modes and same growth rates σ_i are appropriate for the time discretized problem, and furthermore that negative σ_i implies κ less than unity which corresponds to stable time-stepping.

2.3. Splitting Formulation

Uncoupling of the governing equations (2.1) can be obtained by introducing a nondivergent intermediate velocity projection $\mathbf{v}^*$ and corresponding eigenmode $\tilde{\mathbf{v}}^*$. Assuming again a modal decomposition with amplification factor $\tilde{\kappa}$, we obtain

$$\tilde{\mathbf{v}}^* - P(\tilde{\kappa})\,\tilde{\mathbf{v}} = -\nabla p \tilde{\kappa} \Delta t \tag{2.4a}$$

$$\nabla \cdot \tilde{\mathbf{v}}^* = 0 \tag{2.4b}$$

$$\gamma_0 \tilde{\kappa} \tilde{\mathbf{v}} - \tilde{\mathbf{v}}^* = \nu \Delta t R(\tilde{\kappa})\, \nabla^2 \tilde{\mathbf{v}} \tag{2.4c}$$

Elimination of $\tilde{\mathbf{v}}$ followed by an operation with $\nabla \times \nabla$ and using (2.4b) leads to

$$\left[\frac{\gamma_0 \tilde{\kappa} - P(\tilde{\kappa})}{\nu \Delta t R(\tilde{\kappa})} - \nabla^2\right] \nabla^2 \tilde{\mathbf{v}}^* = \left(\frac{\tilde{\sigma}}{\nu} - \nabla^2\right) \nabla^2 \tilde{\mathbf{v}}^* = 0 \tag{2.5}$$

where here we can again define a decay rate $\tilde{\sigma}$ equal to the first term in the square brackets above as before. The final velocity $\tilde{\mathbf{v}}$, however, satisfies a different equation [obtained from (2.4c)] of the form

$$\left(\frac{\tilde{\sigma}}{\nu} - \nabla^2\right) \nabla^2 \left[\frac{\gamma_0 \tilde{\kappa}}{\nu \Delta t R(\tilde{\kappa})} - \nabla^2\right] \tilde{\mathbf{v}} = 0 \tag{2.6}$$

Equation (2.5) suggests that $\mathbf{v}^*$ satisfies an equation similar to the continuous problem equation and thus has two nondivergent modes (the pressure and the time-stepping mode corresponding to the Laplacian and time-dependent operator in the equation, respectively). However, the final velocity $\tilde{\mathbf{v}}$ has an extra mode, due to the last operator in (2.6), producing a numerical boundary layer of thickness $l \propto (\nu \Delta t)^{1/2}$. This mode is responsible for what is typically referred to as *splitting error*. In the following, we analyze the effect of such a splitting error on the accuracy and stability of the overall scheme.

2.4. Analysis of a Two-Dimensional Flow with One Periodic Direction

As a model problem we consider here a time-dependent Stokes flow problem between parallel plates which has been studied before both analytically and numerically (Orszag *et al.*, 1986; Deville, 1984). This problem, although linear, embodies all the essential features of the incompressible Navier–Stokes equations and can serve as a prototype to assess the effect of the treatment of the pressure boundary condition on the overall time-accuracy of the scheme. The choice of the initial conditions is very important as pointed out in Deville (1984) for a unique pressure solution; a compatible initial field is given by

$$\tilde{u} = [\cos \mu \sinh(ky) + \mu/k \cosh k \sin(\mu y)]\, i \tag{2.7a}$$

$$\tilde{v} = [\cos \mu \cosh(ky) - \cosh k \cos(\mu y)] \tag{2.7b}$$

where i is the imaginary unit, and k is the streamwise (x-direction) wave number. Here we consider the case $\nu = 1$ and $k = 1$. All eigenvalues of σ for this system are real and negative, indicating stability.

The x-direction is periodic and we therefore can write the equation for the modes corresponding to wave number k as follows:

$$\mathbf{v}(x, y) = (\tilde{u}(y), \tilde{v}(y))\, e^{ikx} \tag{2.8}$$

From Orszag *et al.* (1986) we get the (symmetric) eigenvalue equation for a nonsplit formulation as follows:

$$k \tanh k = -\mu \tan \mu, \text{ where } \mu^2 = -k^2 - \sigma/\nu \tag{2.9}$$

For the current problem the general operators appearing in (2.4a)–(2.4c) can be rewritten as

$$\nabla^2 = D^2 - k^2, \qquad \nabla^2 - \frac{\tilde{\sigma}}{\nu} = D^2 + \tilde{\mu}^2, \qquad \nabla^2 - \frac{\gamma_0 \tilde{\kappa}}{\nu \Delta t \tilde{R}} = D^2 - \lambda^2 \tag{2.10a}$$

where we have used above the following definitions:

$$\tilde{\mu}^2 = -k^2 - \frac{\tilde{\sigma}}{\nu}, \qquad \lambda^2 = k^2 + \frac{\gamma_0 \tilde{\kappa}}{\nu \Delta t \tilde{R}} \tag{2.10b}$$

$$\tilde{P} = P(\tilde{\kappa}), \qquad \tilde{R} = R(\tilde{\kappa}) \tag{2.10c}$$

$$D = \frac{d}{dy} \tag{2.10d}$$

The general form of the solution $\tilde{v}$, $\tilde{v}^*$ that is symmetric about $y=0$ is

$$\tilde{v}^* = \gamma_0 A^* \cosh ky + \gamma_0 B^* \cos \tilde{\mu} y \tag{2.11a}$$

$$\tilde{v} = \tilde{A} \cosh ky + \tilde{B} \cos \tilde{\mu} y + \tilde{C} \cosh \lambda y \tag{2.11b}$$

We now consider each of the modes (k, μ, λ) separately; the first two are nondivergent as was mentioned earlier. Considering, for example, first the mode k as

$$\tilde{v}_k^* = \gamma_0 A^* \cosh ky, \qquad \tilde{v}_k = \tilde{A} \cosh ky \tag{2.12a}$$

and subsituting in (2.4c) we obtain

$$\tilde{A} = \frac{A^*}{\tilde{\kappa}} \tag{2.12b}$$

The corresponding velocity in the x-direction is obtained from the divergence-free condition

$$\tilde{u}_k = -\frac{D\tilde{v}_k}{ik} = i \sinh ky \frac{A^*}{\tilde{\kappa}} \tag{2.12c}$$

Similarly, we obtain for the second mode the relations

$$\tilde{B} = \frac{\gamma_0 B^*}{\tilde{P}} \quad \text{and} \quad \tilde{u}_\mu = -\frac{i\tilde{\mu}}{k} \tilde{B} \sin \tilde{\mu} y \tag{2.13}$$

Finally, for the nondivergent third mode for which $v_\lambda^* = 0$ we obtain again from (2.4a)

$$-\tilde{P} \mathbf{v}_\lambda = -\tilde{\kappa} \nabla p \, \Delta t \tag{2.14a}$$

and therefore the field $\mathbf{v}_\lambda$ is irrotational, i.e., $\nabla \times \mathbf{v}_\lambda = 0$; this implies that the following relation holds:

$$D\tilde{u}_\lambda = ik\tilde{v}_\lambda \tag{2.14b}$$

To summarize, we can now express the modes $(\tilde{u}, \tilde{v})$ as follows (setting $\tilde{C} = C^*$):

$$\tilde{v} = \frac{A^*}{\tilde{\kappa}} \cosh ky + \frac{\gamma_0 B^*}{\tilde{P}} \cos \tilde{\mu} y + C^* \cosh \lambda y \tag{2.15a}$$

$$\tilde{u} = \frac{iA^*}{\tilde{\kappa}} \sinh ky - \frac{i\gamma_0 \tilde{\mu} B^*}{k\tilde{P}} \sin \tilde{\mu} y + iC^* \frac{k}{\lambda} \sinh \lambda y \tag{2.15b}$$

At this point we can find C^* in terms of A^* by employing the boundary condition at $y = 1$ ($\tilde{u} = \tilde{v} = 0$), i.e.,

$$C^* = -\frac{A^* \cosh k(\tilde{\mu} \tan \tilde{\mu} + k \tanh k)}{\tilde{\kappa} \cosh \lambda[\tilde{\mu} \tan \tilde{\mu} + (k^2/\lambda) \tanh \lambda]} \tag{2.16}$$

Using the exact eigenvalue relation [Eq. (2.9)] and the definition equation (2.10b) we also obtain

$$\tilde{\mu} \tan \tilde{\mu} - \mu \tan \mu = \mathcal{O}\left(\frac{\Delta\sigma}{\nu}\right) \tag{2.17}$$

where we define $\Delta\sigma = \tilde{\sigma} - \sigma$. Substituting this last equation in (2.16) and normalizing appropriately with $\cosh \lambda$ we see that the amplitude C^* of the boundary layer error term is proportional to $\Delta\sigma/\nu$, i.e.,

$$C^* \propto \frac{\Delta\sigma}{\nu} \tag{2.18}$$

This last equation suggests that the error in growth rate that characterizes the time-accuracy of the scheme is directly proportional to the amplitude of the divergent mode.

2.5. Pressure Boundary Condition

A separate substep in solving the Navier–Stokes equations using a splitting formulation is a Poisson-type equation derived from (2.4). The corresponding boundary condition for the pressure can also be found from (2.4) applied at the boundary. This is an exact equation and has the form

$$\tilde{\kappa} \frac{\partial p}{\partial n} = \hat{n} \cdot \nu R(\tilde{\kappa}) \nabla^2 \mathbf{v} \tag{2.19}$$

where we assumed here $\mathbf{v} = 0$ at the boundary; here $\hat{n}$ denotes the unit vector normal to the boundary. However, this relation results in a coupled system since $\nabla^2 \mathbf{v}$ is not known at the pressure step. Progress can be made only if an explicit in time treatment is sought for the velocity involved in (2.19). For example, first-order time-accurate relations can be used, which lead to

$$\tilde{\kappa} \frac{\partial p}{\partial n} = \hat{n} \cdot \nu \nabla^2 \tilde{\mathbf{v}} \tag{2.20a}$$

$$\tilde{\kappa} \frac{\partial p}{\partial n} = -\hat{n} \cdot \nu \nabla \times \nabla \times \tilde{\mathbf{v}} \tag{2.20b}$$

where in the latter equation we also incorporated the incompressibility constraint, i.e., $\nabla \cdot \mathbf{v} = 0$. It follows therefore from (2.4a)–(2.4c) with $\mathbf{v}(y=1)=0$, that the above equations take the following forms (respectively):

$$v^* + v\Delta t D^2 \tilde{v} = 0 \tag{2.21a}$$

$$v^* - ivk\Delta t D\tilde{u} = 0 \tag{2.21b}$$

Substitution of v^*, $\tilde{u}$, $\tilde{v}$ in (2.21a) and (2.21b), respectively, gives

$$A^*\left(\gamma_0 + \frac{v\Delta t k^2}{\tilde{\kappa}}\right)\cosh k + B^*\gamma_0\left(1 - \frac{v\Delta t\tilde{\mu}^2}{\tilde{P}}\right)\cos\tilde{\mu} + C^* v\lambda^2\,\Delta t\cosh\lambda = 0 \tag{2.22a}$$

$$A^*\left(\gamma_0 + \frac{v\Delta t k^2}{\tilde{\kappa}}\right)\cosh k + B^*\gamma_0\left(1 - \frac{v\Delta t\tilde{\mu}^2}{\tilde{P}}\right)\cos\tilde{\mu} + C^* v k^2\,\Delta t\cosh\lambda = 0 \tag{2.22b}$$

To satisfy the boundary conditions $\tilde{u} = \tilde{v} = 0$, therefore, the following determinant [obtained by substitution in (2.21a)] should vanish:

$$\begin{vmatrix} \gamma_0\tilde{\kappa} + v\,\Delta t^2 k^2 & \tilde{P} - \tilde{\mu}^2 v\,\Delta t & \lambda^2 v\,\Delta t \\ 1 & 1 & 1 \\ k\tanh k & -\tilde{\mu}\tan\tilde{\mu} & k^2\dfrac{\tanh\lambda}{\lambda} \end{vmatrix} \tag{2.23}$$

The determinant for the second case (2.21b) has a similar form with the term $\lambda^2 v\,\Delta t$ above replaced by the term $k^2 v\,\Delta t$.

We solve the above determinental equation for the particular case of a second-order stiffly stable-scheme (Karniadakis *et al.*, 1990). The eigenvalue $\tilde{\kappa}$ corresponding to (2.23) agrees with the analytical expansion for κ of the nonsplit scheme up to first-order terms, which implies a reduction of the accuracy order of the overall scheme to order one, despite the second-order time-stepping scheme employed; however, the eigenvalue due to (2.21b) agrees with that of κ to second order. The expansion for the amplification factor, $\tilde{\kappa}$, of the splitting scheme is

$$\begin{aligned} \tilde{\kappa} &= \kappa + \Delta\kappa \\ &= [1 + \sigma\,\Delta t + \sigma^2\,\Delta t^2/2 + \sigma^3\,\Delta t^3/3 + \mathcal{O}(\Delta t^4)] \\ &\quad + [\kappa_1\,\Delta t^2 + \kappa_2\,\Delta t^{5/2} + \kappa_3\,\Delta t^3 + \kappa_4\,\Delta t^{7/2} + \mathcal{O}(\Delta t^4)] \end{aligned} \tag{2.24}$$

where we find that $\kappa_1 = \kappa_2 = 0$ and that the next two coefficients κ_3, κ_4 are given by

$$\kappa_3 = \frac{4\tilde{\mu}^2 v\sigma^2 \sin 2\tilde{\mu}}{\sigma + 3 \sin 2\tilde{\mu}} \tag{2.25a}$$

$$\kappa_4 = \frac{8\sqrt{2}}{3\sqrt{3}} \frac{\tilde{\mu} v^{3/2} k^2 \sigma^2 \cos^2 \tilde{\mu}}{2\tilde{\mu} + \sin 2\tilde{\mu}} \tag{2.25b}$$

We also note that the error in growth rate $\Delta\sigma$ which determines the numarical boundary layer amplitude is given by

$$\Delta\sigma = \kappa_3 \Delta t^2 + \kappa_4 \Delta t^{5/2} + \mathcal{O}(\Delta t^3) \tag{2.26}$$

It is seen therefore that the decay rate $\tilde{\sigma}$ computed using the stiffly stable splitting scheme is accurate to second order in Δt if the rotational boundary condition [Eq. (2.21b)] is employed for the pressure. We also see using (2.26) that the error in the numerical boundary layer is of second order.

In the next section we present numerical results for this simple geometry problem, as well as results for a complex geometry problem that support the theoretical prediction regarding the accuracy of the scheme, and in particular we investigate the effect of the nondivergent mode (mode λ above).

3. NUMERICAL RESULTS

3.1. Simple Geometry Problem

As a first test case we consider the two-dimensional problem with one periodic direction as defined in Section 2.2. The semidiscrete governing equations are discretized further in space by employing a simple second-order center finite-difference scheme with 400 points along the y direction to eliminate spatial errors. We only consider the least stable mode as this is the mode resolved by the direct simulation.

In the following tests the accuracy of the various schemes is examined by computing a decay-rate $\tilde{\sigma}$, which is defined as follows (similarly as in Deville *et al.*, 1984):

$$\tilde{\sigma} = -\frac{1}{vT} \ln \frac{v(y=0, t+T)}{v(y=0, t)} \tag{3.1}$$

where the time period T is taken to be $T = 0.3$; with the above parameters

the energy of the initial field has been reduced by almost five orders of magnitude after the period T.

In Fig. 1 we plot the error in the decay rate $\tilde{\sigma}$ for several schemes corresponding to different integration orders and different type of pressure boundary condition. In general, the improved pressure BC as derived directly from the momentum equation (see Section 2) lead to smaller errors in $\tilde{\sigma}$. The larger errors correspond to the classical splitting scheme with the pressure boundary condition of the form $\partial p/\partial n = 0$. This difference in accuracy has a direct effect on the values of the divergence of the velocity field, as is demonstrated in Fig. 2, where we plot the divergence across the channel (y-direction). The numerical boundary layers induced by the non-divergent (splitting) λ-mode are shown clearly for the zero Neumann pressure BC; however, these errors are eliminated almost entirely if a rotational form of the pressure BC is employed.

To validate the results of the normal mode analysis presented earlier regarding the particular form of the pressure BC [i.e., Eqs. (2.20)] we present in Fig. 3 the divergence profile across the channel at $\Delta t = 10^{-2}$ for two types of pressure BC [curve A: Eq. (2.20a); curve B: Eq. (2.20b)]. Indeed, we verified that a higher-order accuracy associated with the latter BC leads

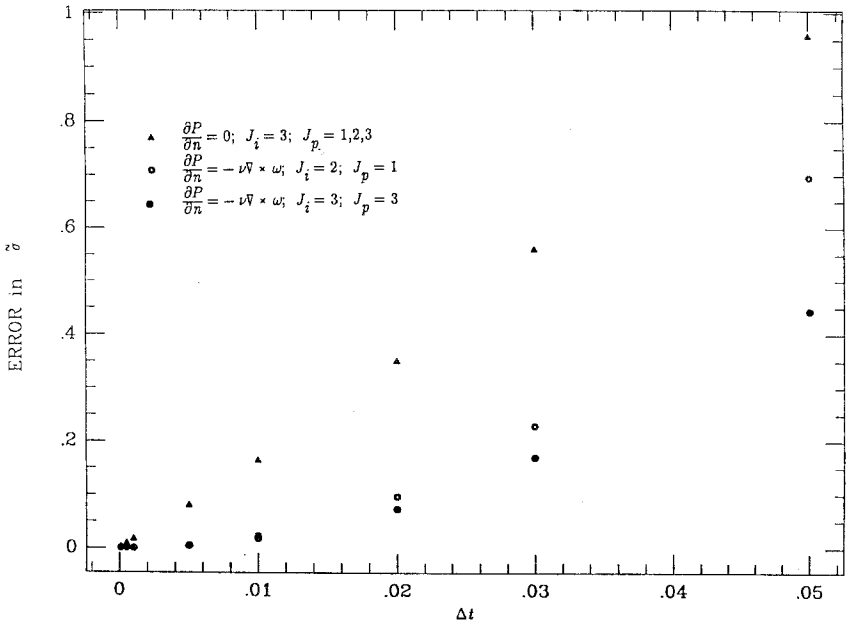

Fig. 1. Error on decay rate $\tilde{\sigma}$ versus time step Δt for different pressure boundary condition and different integration schemes. Here J_i, J_p denote the integration order of the viscous and pressure terms respectively.

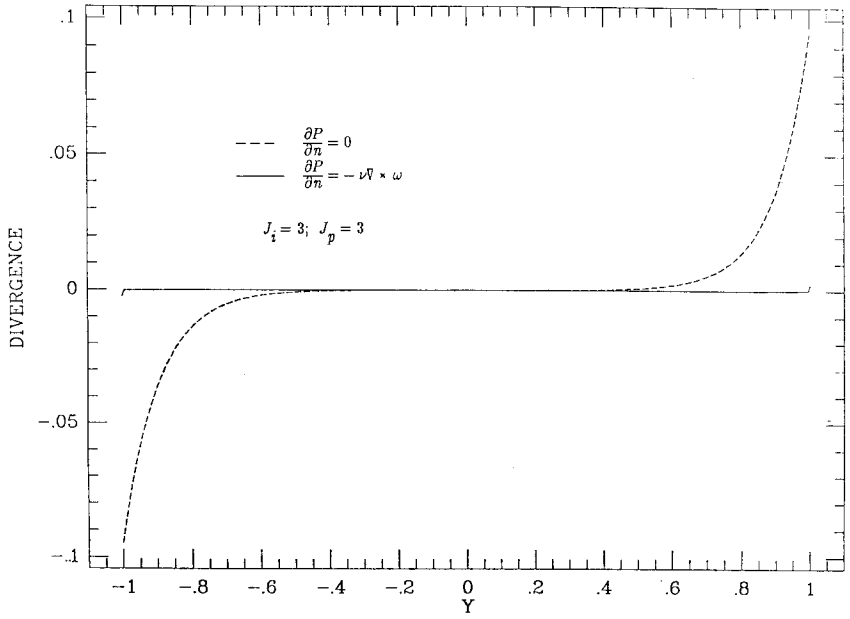

Fig. 2. Divergence of velocity field across the channel. Two very thick (numerical) boundary layers are predicted at the two solid boundaries. Incorporation of the rotational form of boundary condition eliminates completely their boundary layers.

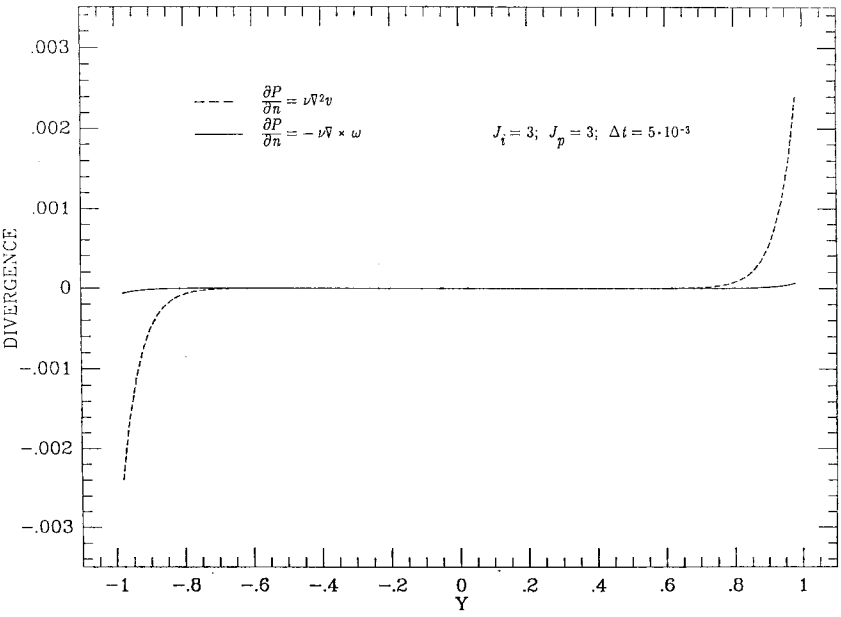

Fig. 3. Comparison of rotational and nonrotational pressure boundary condition. Large divergence errors occur with the nonrotational form, even at small Δt.

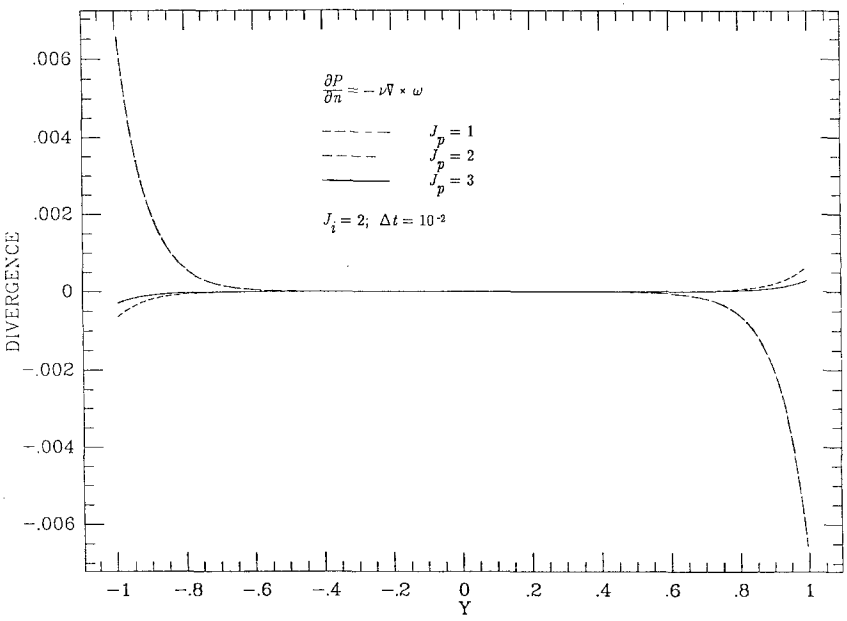

Fig. 4. Effect of the explicit integration order in the pressure boundary condition upon the accuracy of the solution. High-order integration results in negligible errors in velocity divergence.

to almost zero divergence error at the two solid boundaries. This divergence error in its turn varies with the order of the intergration scheme employed as we show in Fig. 4, where we plot the divergence for first-, second-, and third-order schemes. Finally, the direct effect of the time-accuracy on the efficient removal of the boundary divergence errors is shown in Fig. 5, where we present divergence errors versus different time steps. We see that a typical time step $\Delta t = 10^{-2}$ results in divergence errors comparable to the overall spatial discretization errors which are close to machine accuracy for our single-precision computations.

3.2. Complex Geometry Problem

As a second test problem we consider a two-dimensional Stokes flow past a circular cylinder placed next to a moving wall. The available exact solution due to Wannier (1950) for this complex-geometry flow allows for reliable evaluation of the time-differencing error. This problem and its variants have been recently used for code verification purposes (Beris *et al.*, 1984; Korczak and Patera, 1986; Maslanik *et al.*, 1989). The exact solution and the particular parameters we use in the present test are given by

$$u = -\frac{2(A+Fy)}{K_1}\left[(s+y)+\frac{K_1}{K_2}(s-y)\right]-D$$
$$-F\ln\left(\frac{K_1}{K_2}\right)-\frac{B}{K_1}\left[(s+2y)-\frac{2y(s+y)^2}{K_1}\right]$$
$$-\frac{C}{K_2}\left[(s-2y)+\frac{2y(s-y)^2}{K_2}\right] \tag{3.2a}$$

$$v=\frac{2x}{K_1K_2}(A+Fy)(K_2-K_1)-\frac{2Bxy(s+y)}{K_1^2}-\frac{2Cxy(s-y)}{K_2^2} \tag{3.2b}$$

where we define:

$$A=-\frac{Ud}{\ln(\Gamma)}-\frac{dRu}{2s}, \qquad B=\frac{2(d+s)\,U}{\ln(\Gamma)}+\frac{(d+s)\,RU}{s} \tag{3.3a}$$

and

$$C=\frac{2(d-s)\,U}{\ln(\Gamma)}+\frac{(d-s)\,Ru}{s}, \qquad D=-U, \qquad F=\frac{U}{\ln(\Gamma)} \tag{3.3b}$$

$$K_1=x^2+(s+y)^2, \qquad K_2=x^2+(s-y)^2$$

$$s^2=d^2-R^2, \qquad \Gamma=\frac{d+s}{d-s} \tag{3.3c}$$

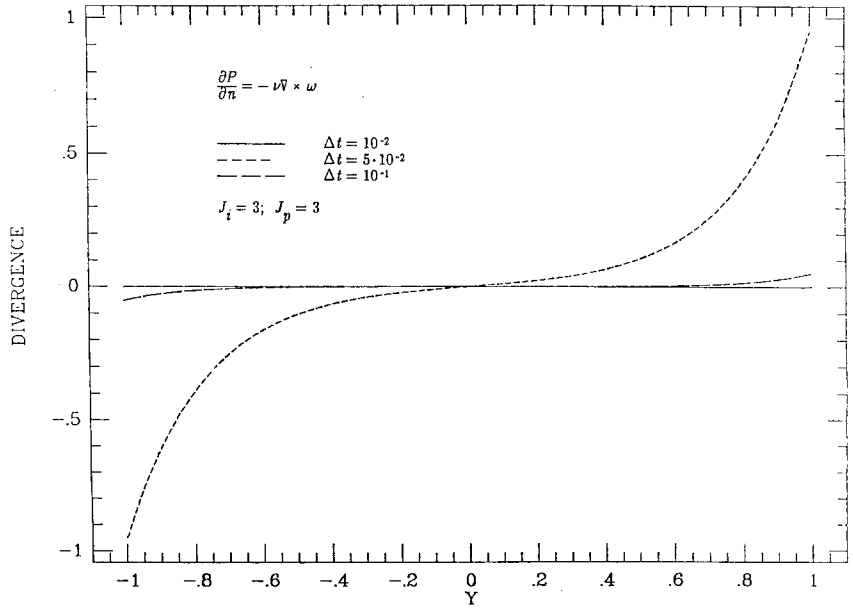

Fig. 5. Effect of time step Δt on the velocity divergence errors. High-order schemes induce minimal divergence error at modest values of Δt.

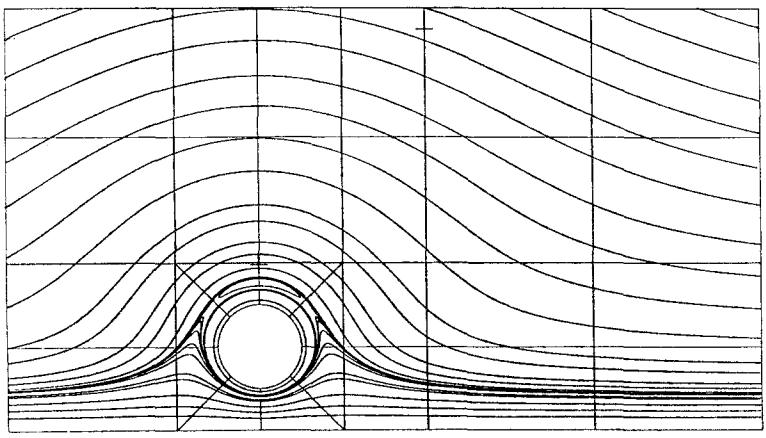

Fig. 6. Steady-state streamlines for the Stokes flow. The discretization is based on spectral element methods.

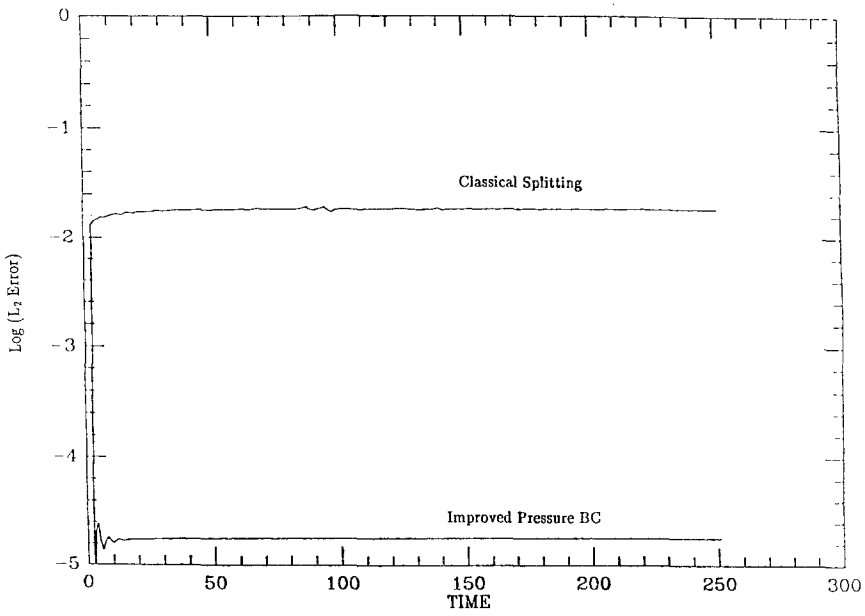

Fig. 7. L_2-error history at a fixed point in the computational domain indicating a three-orders-of-magnitude increase in accuracy for the improved pressure boundary condition.

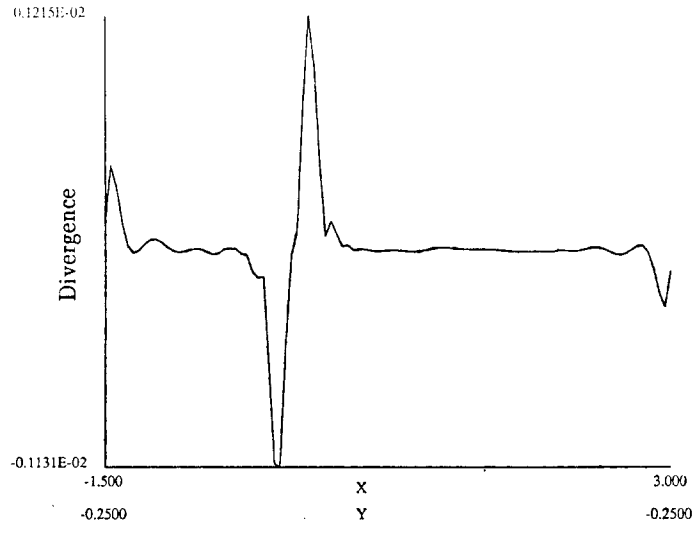

(a)

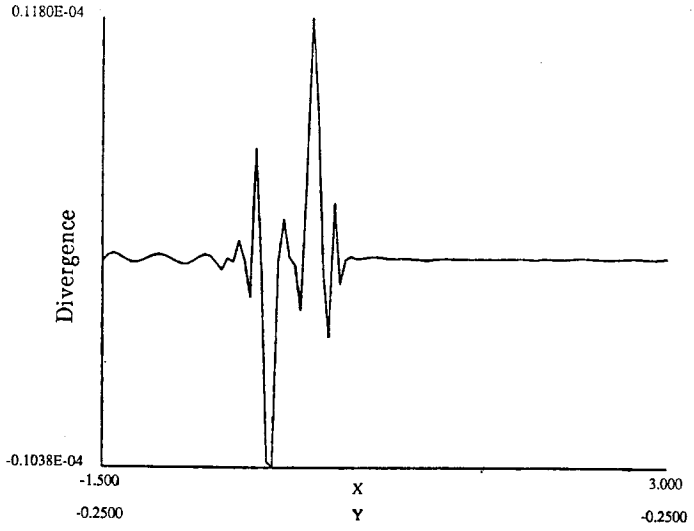

(b)

Fig. 8. Velocity divergence errors at $y = -0.25$, where maximum errors occur. (a) Classical splitting scheme. (b) High-order splitting scheme.

Here, we denote by $R = 0.25$ the cylinder radius, by $d = 0.5$ the distance of the cylinder center from the wall, and by $U = 1$ the velocity of the moving wall; the cylinder is also spinning in the direction of the moving wall at velocity $u = 0.5$. The discretization employed for this simulation is based on the spectral element methodology, which provides high spatial accuracy for complex geometry flows and smooth solutions (Karniadakis, 1989). Dirichlet BC were used at the boundaries of the truncated domain computed from the exact solution. The computed steady-state solution is shown in Fig. 6 in the form of streamlines, and is indistinquishable from the exact solution. In Fig. 7 we plot the convergence history to the final steady state presented as the L^2-error at $\Delta t = 10^{-2}$ versus time for two different schemes: (A) the classical splitting scheme using the inviscid-type pressure BC; and the new stiffly stable schemes corresponding to (B) third-order. The superiority of the new pressure boundary condition is reflected in the difference between curves (A) and (B).

To test how accurately the incompressibility constraint is honored in this simulation we plot in Figs. 8a and 8b the divergence profile across a line very close to no-slip boundaries (see Fig. 6), where the divergence achieves its maximum value. The first plot corresponds again to the classical splitting scheme and is characterized by the relatively large divergence value $\mathcal{O}(10^{-3})$ as well as two pronounced boundary layers at the two ends of the domain. In Fig. 8b, however, which corresponds to a simulation with the improved rotational pressure BC the divergence is smaller by two orders of magnitude, while the numerical boundary layers have been eliminated completely. These results therefore agree with the results of the simple geometry simulation and are consistent with the findings of the normal modes analysis presented in Section 1.

4. CONCLUSIONS

Our findings in this work validate the new splitting method proposed in Karniadakis *et al.* (1990) for the solution of the incompressible Navier–Stokes equations; in particular, a time accuracy of a specified high order is readily achieved without introducing any extra coupling between pressure and velocity equations (Rønquist, 1988), which would result in prohibitively expensive calculations. In addition, the boundary-divergence errors that are present in the classical splitting method are completely eliminated using the improved, rotational Neumann boundary conditions for the pressure.

ACKNOWLEDGMENTS

Financial support for the current work was provided by grants from NSF (CTS-8906911 and CTS-8906432), DARPA contract No. N00014-86-K-0759, and ONR contract No. N00014-82-C-0451. One of us (M.I.) would like to acknowledge the support of a fund for the promotion of research at the Technion.

REFERENCES

Beris, A. N., Armstrong, R. C., and Brown, R. A. (1984). Finite element calculation of viscoelastic flow in a journal bearing: small eccentricities, *J. Non-Newtonian Fluid Mech.* **16**, 141.

Deville, M. O., Kleiser, L., and Montigny-Rannou, F. (1984). Pressure and time treatment for Chebyshev spectral solution of a Stokes problem, *Int. J. Num. Methods Fluids* **4**, 1149.

Karniadakis, G. E. (1989). Spectral element simulations of laminar and turbulent flows in complex geometries, *Appl. Num. Math.* **6**, 85.

Karniadakis, G. E., and Triantafyllou, G. S. (1989). Frequency selection and asymptotic states of laminar wakes, *J. Fluid Mech.* **199**, 441.

Karniadakis, G. E., Mikic, B. B., and Patera, A. T. (1988). Minimum dissipation transport enhancement by flow destabilization: Reynolds' analogy revisited, *J. Fluid Mech.* **192**, 365.

Karniadakis, G. E. Israeli, M., and Orszag, S. A. (1990). High-order splitting methods for the incompressible Navier–Stokes equations, *J. Comput. Phys.*, submitted, 1989.

Kim, J., and Moin, P. (1985). Application of a fractional-step method to incompressible Navier-Stokes equation, *J. Comput. Phys.* **59**, 308.

Korczak, K. Z., and Patera, A. T. (1986). An isoparametric spectral element method for solution of the Navier-Stokes equations in complex geometry, *J. Comput. Phys.* **62**, 361.

Marcus, P. S. (1984). Simulation of Taylor–Couette flow. Part 1. Numerical methods and comparison with experiment, *J. Fluid Mech.* **146**, 45.

Maslanik, M. M., Sani, R. L., and Gresho, P. M. (1989). An isoparametric finite element Stokes flow test problem, to appear in *Comm. & Appl. Num. Methods.*

Orszag, S. A., and Kells, L. C. (1980). Transition to turbulence in plane Poiseuille flow and plane Couette flow, *J. Fluid Mech.* **96**, 159.

Orszag, S. A., Israeli, M., and Deville, M. O. (1986). Boundary conditions for incompressible flows, *J. Sci. Comput* **1**(1), 75.

Rønquist, E. M. (1988). Optimal spectral element methods for the unsteady three-dimensional incompressible Navier–Stokes equations, Ph.D. thesis, Massachusetts Institute of Technology, 1988.

Wannier, G. H. (1950). A contribution to the hydrodynamics of lubrication. *Quart. Appl. Math.* **8**, 1.

Yanenko, N. (1971). *The Method of Fractional Steps*, Springer, New York.

Zang, T. A., and Hussaini, M. Y. (1986). On spectral multigrid methods for the time-dependent Navier–Stokes equations, *Appl. Num. Math.* **19**, 359.

Printed in Belgium